A R C H I V E S O F M E T A L L U R G Y A N D M A T E R I A L S
Volume 55 2010 Issue 4
DOI: 10.2478/v10172-010-0003-7

H. PAUL[*] [**], M. DARRIEULAT[***], N. VANDERESSE[***], L. LITYŃSKA[*], M. MISZCZYK[*]

MICROSTRUCTURE OF WARM WORKED ZIRCALLOY-4

MIKROSTRUKTURA STOPU ZIRCALL0Y-4 PRZETWARZANEGO W PODWYŻSZONYCH TEMPERATURACH

The microstructure of commercial purity Zircalloy-4 (Zry-4) compressed at temperatures 650°C and 750°C up to strains of 0.8 was characterized over a wide range of scales, using optical metallography, scanning (SEM) and transmission (TEM) electron microscopy. The typical microstructure after warm deformation consisted of the α-phase matrix and the second phase particles (SPP) enriched in Fe and Cr. Two kinds of these particles were observed. The large isolated SPP were situated along boundaries of lamellae of α-phase, whereas very fine intermetallic particles were nearly homogeneously distributed inside the lamellae.

The intensity of recrystallization was main factor deciding on microstructure development in this material. The efficiency of that process increased quite rapidly with temperature or decreasing strain rate. The appearance of twins was the second important feature of the 'warm deformed' structure with the prevailing $\{1\bar{1}02\}$ – type system of twins. They were occasionally observed in all samples after the deformation at 650°C and 750°C temperatures.

Keywords: Zircalloy-4, microstructure, twinning, second phase particles, hot deformation

W pracy dokonano wieloskalowej charakterystyki mikrostruktury stopu Zircalloy-4 przerabianego plastycznie w zakresie pośrednich temperatur, tj. 650°C-750°C, w zakresie odkształceń logarytmicznych do 0.8, z wykorzystaniem technik mikroskopii optycznej oraz skaningowej i transmisyjnej mikroskopii elektronowej. W obrazie mikrostruktury obserwowano płytki fazy α oraz wydzielenia cząstek drugiej fazy wzbogaconoej w Fe oraz Cr. Obserwowano dwa typy wydzieleń. Duże izolowane cząstki usytuowane były wzdłuż granic płytek fazy α, podczas gdy wydzielenia dyspersyjne rozmieszczone były równomiernie w strukturze stopu. Głównym parametrem który decydował o zróżnicowaniu w strukturze stopu była intensywność zachodzenia procesu rekrystalizacji, która silnie uzależniona była od temperatury i prędkości odkształcenia. Drugim istotnym zjawiskiem obserwowanym po odkształceniu w obydwu temperaturach było pojawienie się obszarów zbliźniaczonych, przy czym dominował system zbliźniaczenia na płaszczyźnie $\{1\bar{1}02\}$

1. Introduction

Zircalloy-4 (Zry-4) is one of the most popular materials in nuclear applications based on zirconium. It is characterized by complex structure of precipitates, which are known to play an important role in the macroscopic properties, i.e. strength, ductility, stiffness, strain rate sensitivity and resistance of the material to corrosion (e.g. Crépin et al., 1995; Logé et al., 2000; Chauvy et al., 2006).

The processing ability of the alloy is governed by the microstructure formed at different stages of its working. One of the routes to increase the toughness and ductility is a hot forging in the β-range (1000°C – 1050°C), water quenching from the homogeneous β-phase (above 1000°C), forging and rolling or extrusion at intermediate temperatures (so-called upper α-range ranging from 650°C to 780°C). Finally, a series of cold rolling followed by intermediate anneals in vacuum furnaces (Lemaignan & Motta, 1992) are commonly applied. Another way to improve ductility is to apply β-quenching from temperature close to 1000°C just before the cold work operation followed by annealing at temperature close to the upper boundary of the α-region (usually 600°C). The two-phase field extends approximately from 980°C to 810°C, during which colonies of hexagonal close packed (hcp) α-phase appear. They are basically single crystals. The Fe and Cr, dissolved up to of 0.21 and 0.11 in the β-phase, are neither soluble in

[*] INSTITUTE OF METALLURGY AND MATERIALS SCIENCE, PAS, KRAKÓW, POLAND
[**] OPOLE UNIVERSITY OF TECHNOLOGY, MECHANICAL DEPARTMENT, POLAND
[***] ECOLE DES MINES DE SAINT ETIENNE, CENTRE SMS, FRANCE

the α-phase nor in precipitate along parallel planes. The generic formula of these large, second phase precipitates (SPP) is $(Fe_xCr_{(1-x)})Zr_2$ (Lemaignan & Motta, 1992).

Since final shaping of tubes or flat products is realized within upper α-range the macroscopic properties are influenced by the microstructure and the texture changes occurring within α-phase. The main features of the deformation at high temperatures within upper α-field are already known, e.g. Chauvy, (2004), Chauvy et al., (2006). The material obtained after quenching from the β-domain is well known to exhibit a Widmanstätten-type structure consisting of α-phase platelets organised either into parallel colonies or basket wave tangles (Chauvy et al., 2006). Its needles or lamellae sometimes are referred as laths. In the β-phase field, the body centred cubic (bcc) grains are large, i.e. extend up to few mm. Most of the laths are distorted and take kinked shapes. Their crystallographic orientations, initially identical within a given colony, 'grow' progressively apart. Subgrains and grain boundaries develop through them, so that smaller, roughly equiaxed grains replace the laths (globularization).

The identification of the deformation mechanisms valid in α-range constitutes one of the most important problems. In pure zirconium and Zr-alloys (as in all hexagonal metals) twinning is an important deformation mode and at low homologous temperatures, the deformation takes place through a mixture of slip and twinning (e.g. Tome et al., 1991; Song & Gray III, 1995). The twinning activity and the associated creation of twin domains inside the grains lead to rapid texture evolution and to a characteristic increase of hardening rate. The twinned volume fraction increases with strain and deformation rate and decreases with temperature (Christian & Mahajan, 1995). Earlier works on pure Zr and Zr-alloys deformed at high temperature neglected twinning and considered that mechanism to occur mainly at room temperature. However, Fundenberger et al., 1990, observed a more complex variation of the twins density with temperature. The authors showed the increase of twin fraction with temperature in alloys, in which the alloying elements are in substitution in the matrix, i.e. Sn (Zy-4) or Hf (Zr-Hf). The same investigations showed that in tension or biaxial expansion tests only the $\{0\bar{1}2\}$ and the $\{1\bar{2}2\}$-types of twinning occured. Additionally, the Zr-alloys with high oxygen contents displayed much smaller twinned volume fraction, independently on the temperature of the test. Other controversial problems are related to morphology of precipitations, their crystallographic relation to the matrix or identification of the preferential planes of precipitation.

The aim of the present work has been to evaluate the influence of temperature within intermediate regime during deformation on the dislocation structure evolution of the Zry-4 alloy and identification of the active deformation mechanisms. In particular, a validity of deformation twinning in samples deformed at 650°C and 750°C is of special interest. To enlarge the hardening effect in samples deformed at lower temperature, higher strain rate was applied. In the case of samples deformed at higher temperature, very low strain rate was applied to facilitate the recovery and recrystallization effects. This work has concentrated on transmission electron microscopy (TEM) studies of dislocation microstructure development, changes in chemical composition and crystallographic orientation analysed by TEM orientation mapping. The uniaxial compression and plane strain deformation modes were used as a representation of the deformation paths along different surfaces of the extruded tubes.

2. Experimental procedures

A standard polycrystalline Zry-4 alloy with the chemical composition presented in Table 1 was selected for the examination. The material was supplied in the form of plate obtained by rolling in the $\alpha + \beta$ two phase range and annealed in the β domain at 1020°C before quenching. The microstructure before deformation can be described by large β grains (mostly 700 μm in size) which split into a certain number of α grains, referred to as colonies. The colonies had different crystallographic orientations. The shape of the colonies was a bit intricate and far from the semi-ellipsoidal form, often cited in literature (Crépin et al., 1995; Chauvy et al., 2006).

In the case of uniaxial compression the specimens were machined with their axis parallel to the rolling direction whereas in the case of channel-die compressed samples the coordinate system of rolled sheet was retained. In both tests, the samples were deformed at 650°C and 750°C up to logarithmic strain of 0.8 at a nominal strain rate ranged between 10^{-2} s^{-1} – 1.0 s^{-1} using graphite as lubricant. After deformation, the specimens were water quenched to freeze the microstructure.

TABLE

Chemical composition of Zircalloy-4 (Zr: balance)

Alloying elements (wt.%)	Sn	Cr	Fe	Cr + Fe	O (ppm)	Si (ppm)
Standard Zy-4	1.2-1.7	0.07-0.33	0.18-0.24	0.28-0.37	900-1600	120
Zy-4 (this work)	1.3	0.10-0.11	0.22-0.24	~0.32	1000-1400	~100

In the case of channel-die compressed samples the specimens for detailed TEM investigations were cut perpendicular to the transverse direction (TD), whereas in the case of uniaxially compressed samples – parallel to the compression axis. Next step was mechanical grounding with SiC papers. Finally, the TEM thin foils were prepared by a twin-jet technique using TenuPol-5. An electro-polishing solution consisting of 470 ml methanol, 30 ml sulphuric acid, and 1.2 ml hydrofluoric acid was used at a voltage of 21-22 V and a temperature within the range of (-)35°C - (-)30°C. The microstructure observations and chemical analyses were performed on a FEI Technai G^2 microscope with field emission gun equipped with EDAX energy dispersive X-ray spectrometer (EDS) and high angle angular dark field (HAADF) detector, operating at the accelerating voltage of 200 kV. The crystal structure of the particles was determined by the selected area diffraction technique. About 20 particles of different size were evaluated by EDS.

The detailed microstructure/microtexture evolution during deformation was analysed by systematic local orientation measurements (orientation mapping) in a TEM using a step size between 10 to 35nm. The local orientations were characterized by TEM using a 200kV PHILIPS CM200 with automated Kikuchi line based system. Details of the acquisition of diffraction patterns, image corrections, line detection and indexing were described elsewhere (Morawiec, 1999; Paul, 2010). The post-processing analysis of the orientation maps was performed using HKL Technology Channel 5 software.

3. Results and discussion

3.1. Global microstructure development

The observations at optical (OM) and scanning electron (SEM) microscopes scales clearly shows lamellae microkinking in the microstructure. This is visible after straining in both deformation tests especially when the compression axis is close to the platelet plane. Independently of the applied deformation conditions, the observed microstructures do not exhibit any visible hardening, as reported previously by Chauvy et al., (2006). The typical microstructure of β-quenched material is composed of basket wave α-grains appeared from the former β-grains. Figure 1 shows the OM and SEM

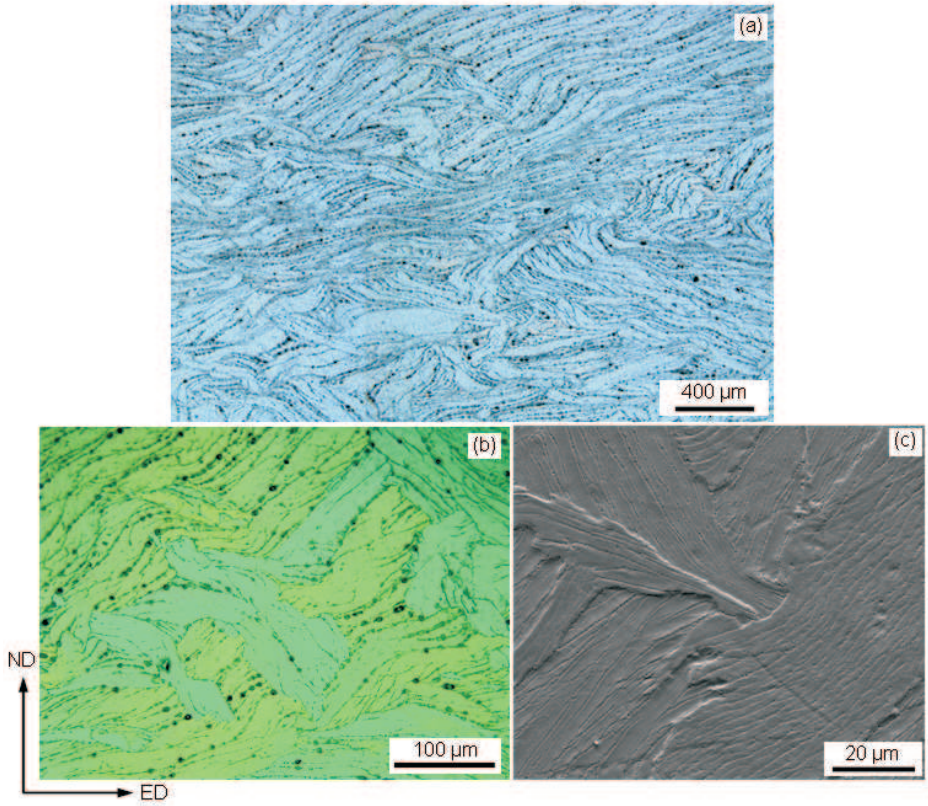

Fig. 1. Typical microstructure of β-quench material after plane strain compression. (a) Optical micrographs showing laths microkinking. Analyses at larger magnification show localization of precipitates in lath boundaries; (b) microstructure after electrolytic polishing observed under polarized light in optical microscopy and (c) SEM observations in secondary electrons. The contrast obtained in polarized light shows different orientations of the α-grains. Sections perpendicular to TD. Sample deformed up to 0.2 (logarithmic strains) at 750°C and strain rate $1s^{-1}$

microstructures observed in longitudinal section, i.e. ND-ED (where: ND and ED - normal and expansion directions, respectively) of the sample deformed 0.5 in channel-die at 750°C and strain rate of 0.01 s^{-1}. The large second phase particles (LSPP) are located at α-grain boundaries and visible as small black dots.

The platelets that occupy different volumes of uniaxial or channel-die compressed samples generally rotated towards the compression plane, as is visible in Fig. 2a. However, within volumes occupied by the macroscopic shear bands (MSB) an opposite rotation tendency is observed especially well visible within channel-die deformed samples close to the sample corners. This tendency directed the platelets to coincide with macroscopic shear plane inclined at 35-40° to the compression plane (Fig. 2b).

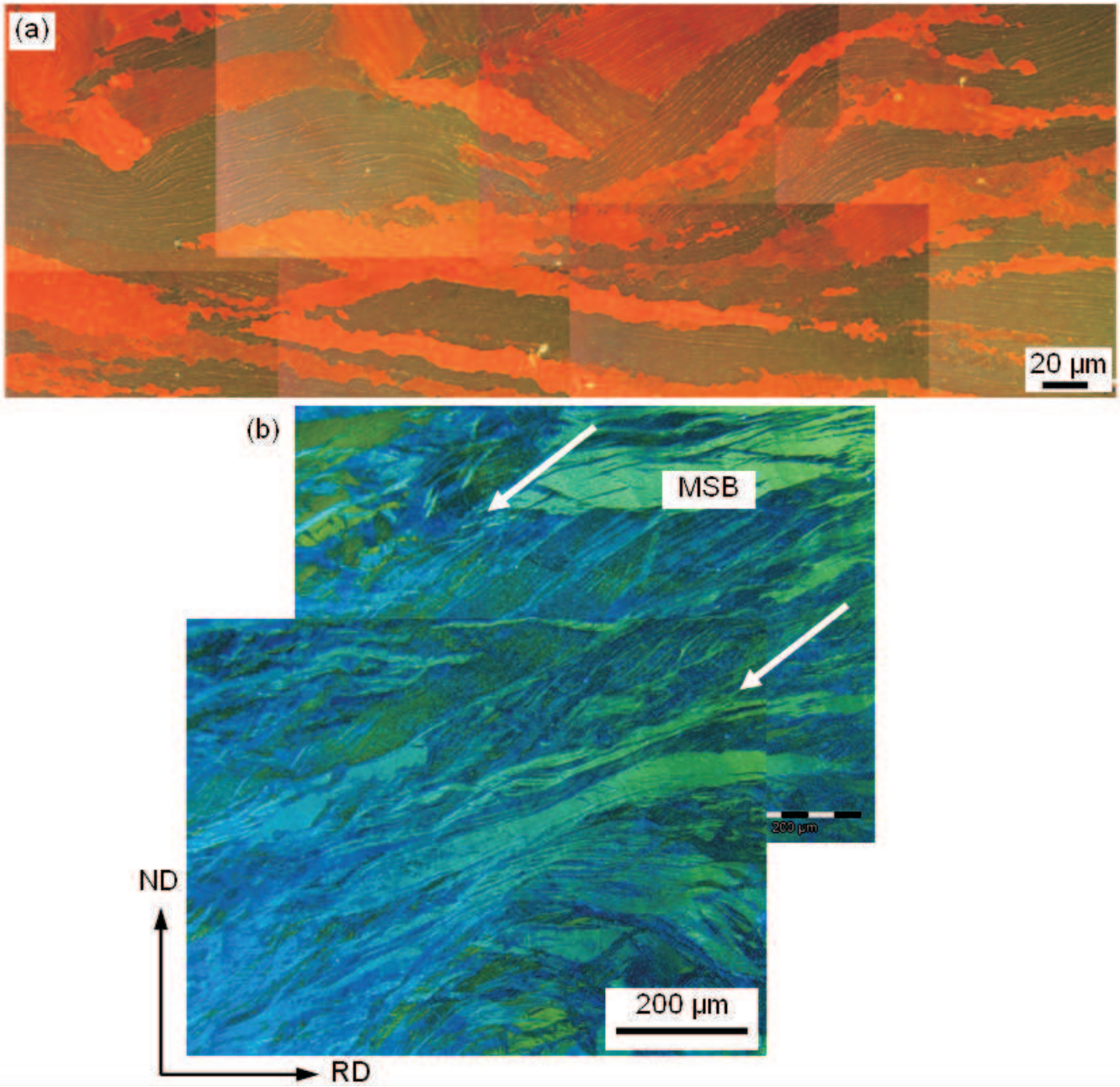

Fig. 2. Different rotation tendencies of platelets observed in uniaxially compressed samples. (a) Rotation towards compression plane and (b) rotation towards shear plane within macroscopic shear bands. Sample deformed up to 0.8 at 650°C and strain rate of 1.0s^{-1}. Plane parallel to the compression direction || ND (where: RD and ND are radial and normal directions, respectively. MSB – macroscopic shear bands) observed with optical microscopy technique

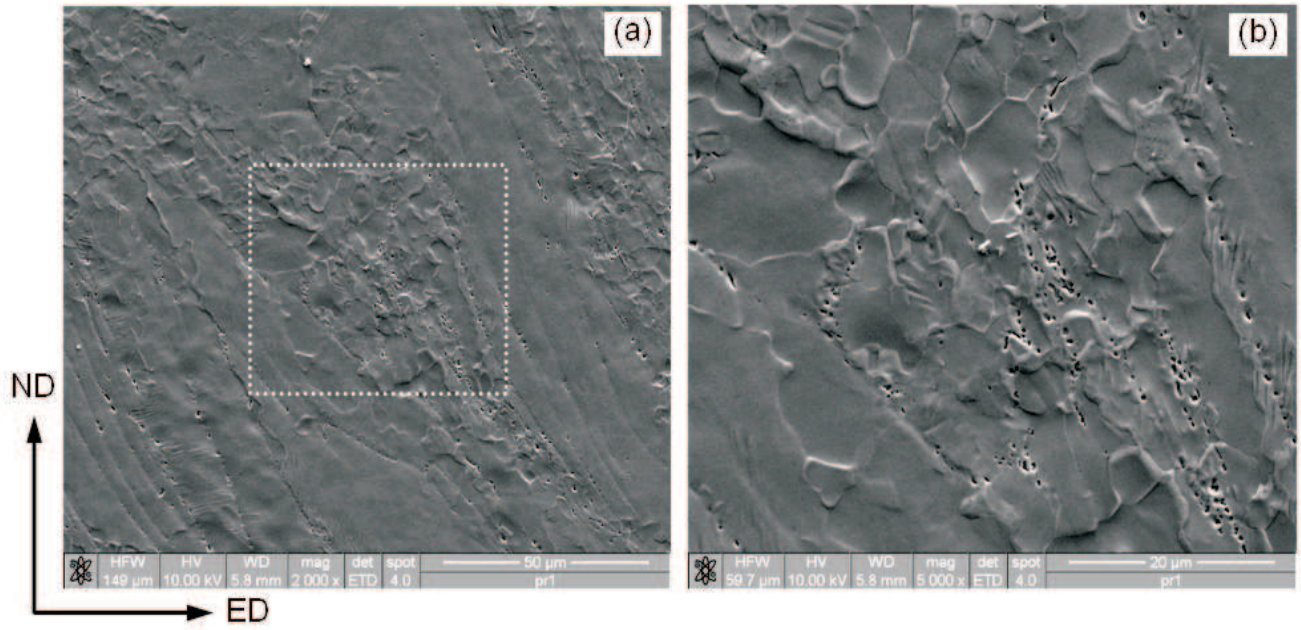

Fig. 3. Beginning stage of recrystallization in near surface region of the sample deformed at 750°C and strain rate of $0.01s^{-1}$. Microstructure observed by using SEMFEG in secondary electrons on sample deformed up to logarithmic strains of 0.5 in channel-die

The dynamic recovery or even recrystallization takes place inside these volumes, as a result of high strain localization. This is especially clearly visible in corners of the samples, deformed in channel-die at 750°C and strain rate of 0.01 s^{-1}. Such volumes (in which deformation seems to be strongly localized) were the first to globularize. Many colonies have been transformed from elongated into small equiaxed grains, of 10 μm in diameter, leading to a refined and more or less homogeneous microstructure (Fig. 3a and b), but some of them remain almost undeformed.

3.2. The identification of the second phase particles

The typical microstructure of the Zry-4 alloy after warm deformation observed at TEM scale consisted of the α-phase and the intermetallic precipitates enriched in Fe and Cr. TEM bright field imaging at low magnification shows very similar microstructure to that observed using OM and SEM. It shows the microstructure composed of laths of α-grains, of different orientation with respect to the external directions with boundaries marked by large second phase particles (LSPP). More detailed analysis at a higher magnification show that two general kinds of precipitates are observed (Fig. 4a). The precipitation of LSPP, take place mostly along parallel planes, and divides α-grains into lamellae. These particles are only rarely observed inside the platelets. The lamellae of the same colony have usually the same crystallographic orientations.

The LSPP showed varied morphologies including near spherical, polygonal, rectangular and square ones. However, most observed particles were rectangular and polygonal (Fig. 4b), as observed earlier by Crépin et al. (1995) and Chauvy et al. (2006). The typical sizes of LSPP ranged between 100-150 nm in length and up to ~70 nm in width. Within particular lamellae of the α-phase, a network of another type of homogeneously distributed intermetallic precipitates was observed (Fig. 4c). The diameter of fine, nearly equiaxed, second phase particles (FSPP) were significantly below 10 nm in diameter.

From the point of view of grain orientations, the basal poles close to the normal of the foil were found in regions exhibiting fine and homogeneously distributed precipitates. The regions with large and isolated particles had more scattered orientations.

The chemical composition of LSPP and neighbouring matrix are presented in Fig. 5. Bright elongated areas indicate increased concentration of the heavy elements (Cr and Fe). The microchemical and crystallographic analyses (selected area diffraction) helped to identified the particles to be of fcc type or quite occasionally a hexagonal Laves-phase of Zr(Fe,Cr)2 type. This is in accordance with Xiao & Ma (1998) statement that $Zr(Cr,Fe)_2$ – type precipitates in Zry-4 alloy quenched from the β-phase have a fcc structure which evolves with subsequent annealing towards the hcp structure. The quantitative analysis shows that the iron to chromium ratio for the LSPP varies from 1.4 to about 2.2, while Tang et al (1996) estimated it as 1.53-2.47. It is possible that some atoms of the Fe and Cr remain in solid solution. However, their concentrations in the matrix are too low to be detected by a standard EDX TEM quantitative microanalysis.

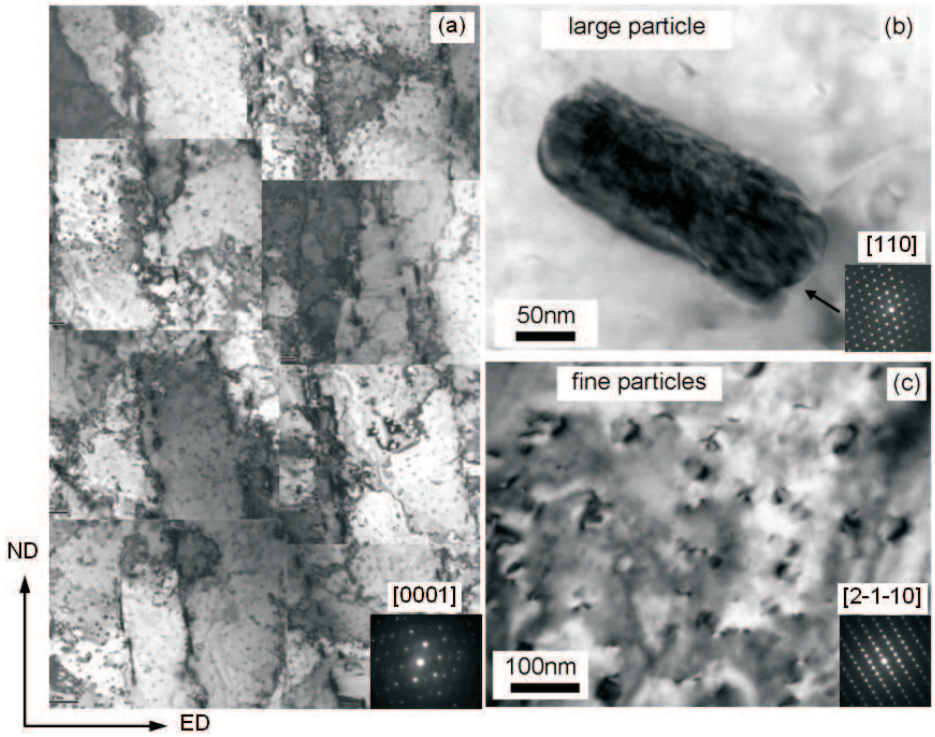

Fig. 4. Typical microstructure of β-quenched material. (a) TEM bright field image showing lamellar microstructure within α-grain; (b) morphology of large particles at lamellae boundary within α-grain, and (c) uniform distribution of fine particles inside lamellae. Selected area diffractions attached to corresponding bright field images indicate beam direction of B=[011] (fcc) and B=[$2\bar{1}\bar{1}0$] (hcp) for large particle and matrix containing small particles, respectively. Sample deformed in channel-die at 650°C up to logarithmic strains of 0.1

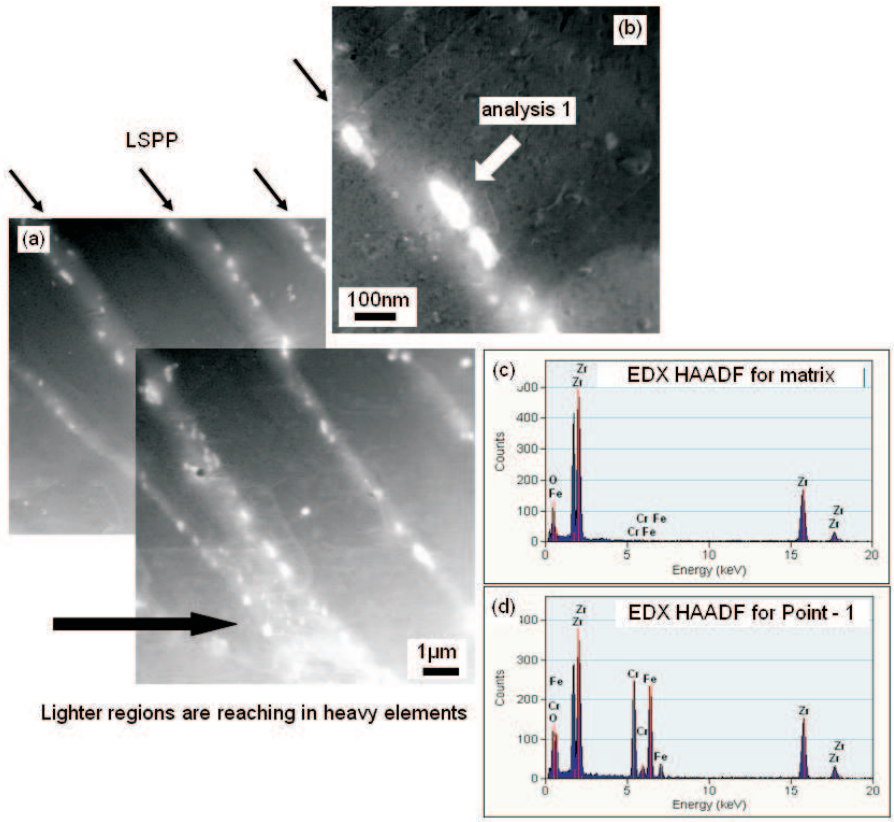

Fig. 5. (a) STEM-HAADF image showing differences in chemical composition of elongated areas where the large particles appeared, (b) a detail from (a), (c) and (d) EDX microanalyses for matrix and particle (point 1). Sample compressed at 750°C up to strains of 0.2

According to Massih et al. (2003), the Fe and Cr alloying elements are in the solid solution within the range of the β-phase. As the temperature is lowered the homogeneous solid solution in the β + α phase becomes metastable and leads to the nucleation and growth of the second phase. The precipitates appear from the β-phase during cooling because of very low solubility of Fe and Cr in the α-phase. As the latter transformations proceed, iron atoms diffuse into $Zr(Cr,Fe)_2$ precipitates (with diameter below 10 nm) and a second type of iron rich, fine particles appear at the same time. The studies of Logé et al. (2000) leads to the conclusion that the FSPP homogeneously distributed in the α-grains are such that the mean diffusion length of iron atoms, released from the precipitates, is comparable to the average precipitate spacing. The average precipitates spacing in this investigation was below 100 nm. Moreover, as it was found by Lemaignan & Motta (1992) the size and coarseness of the particles depended mainly on the degree of matrix supersaturation and the interfacial energy, i.e. the higher the interfacial energy, the stronger the driving force for particle coarsening, as reported by Tang et al. (1996) and Schaffer et al. (1995).

3.3. The development of dislocation structure

Typical dislocation microstructures observed in samples deformed at 650°C and 750°C are shown in Figs. 6 and 8. The analysis shows that independently on the applied deformation mode or strain rate the samples deformed at both temperatures are characterized by similar dislocation arrangements. Additionally the microstructures were very inhomogeneous. The main factor that decides about this differentiation was the intensity of the recrystallization process. In accordance with earlier work by Chauvy et al., (2006) on the same type alloy, at temperatures higher than 650°C, flow stress softening occurs as soon as the yield stress is reached. This effect is due to the dynamic recovery and the efficiency of this process increases quite rapidly with increasing temperature or decreasing strain rate.

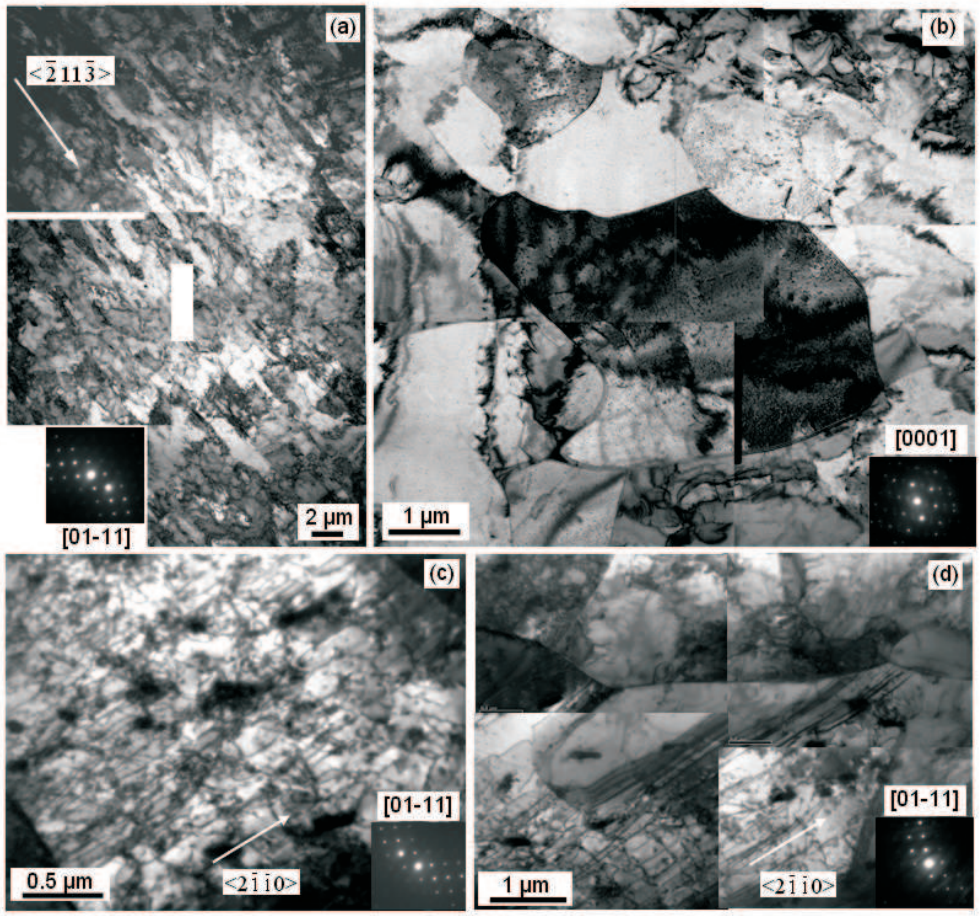

Fig. 6. Bright field TEM microstructures in samples deformed up to 0.8 in uniaxial compression. Dislocation arrangements observed in samples deformed at: (a) and (b) 650°C and strain rate of $1s^{-1}$, (c) and (d) 750°C and strain rate of $0.01s^{-1}$. Differently oriented recrystallized grains with network of small particles are observed in (b). Micrographs in (a), (c) and (d) taken with $[01\bar{1}1]$ whereas in (b) taken with [0001] beam directions (central part), respectively

TEM inspection of the thin foils prepared from the samples uniaxially compressed at 650°C and strain rate of 0.1 s^{-1} shows (Fig. 5a) the dominance of typical as-deformed structure with dislocations formed walls aligned along preferred directions. The dislocations are arranged mainly in 'diffuse', roughly rectangular cells. However, in some cases the dislocations are also observed in the interior of cells. This indicates that inside these volumes no recrystallization or recovery took place during or after deformation. The analysis based on the selected area diffraction shows the foil orientation to be close to the $B = [01\bar{1}0]$ crystallographic direction. The dislocation walls are aligned in $<\bar{1}\bar{1}23>$ direction; this can suggests activation of pyramidal slip systems operating in $\{01\bar{1}1\}$-type planes. However, other volumes of the same sample showed a non-negligible volume fraction of recrystallized areas, as seen in Fig. 7b. The diameter of new grains was less than 2-5 μm. At higher temperature of deformation (i.e. 750°C and very low strain rate of 0.01 s^{-1}) the microstructure is composed of nearly homogeneously distributed single dislocations and the recrystallized areas, characterized by nearly equiaxed, dislocations free new grains.

The dislocation density was significantly smaller in that case with respect to the microstructures observed at 650°C. In some cases individual straight segments of dislocations or dislocations forming diffused networks, i.e. honeycomb shapes of dislocation networks, were observed. Typical dislocation microstructures are presented in Figs. 7c and d. These bright field images were taken with a $[01\bar{1}1]$ beam direction showing relatively straight, elongated lines aligned parallel to $<0\bar{1}\bar{1}2>$ direction. The dislocation interactions and a tendency towards formation of dislocation network were also observed.

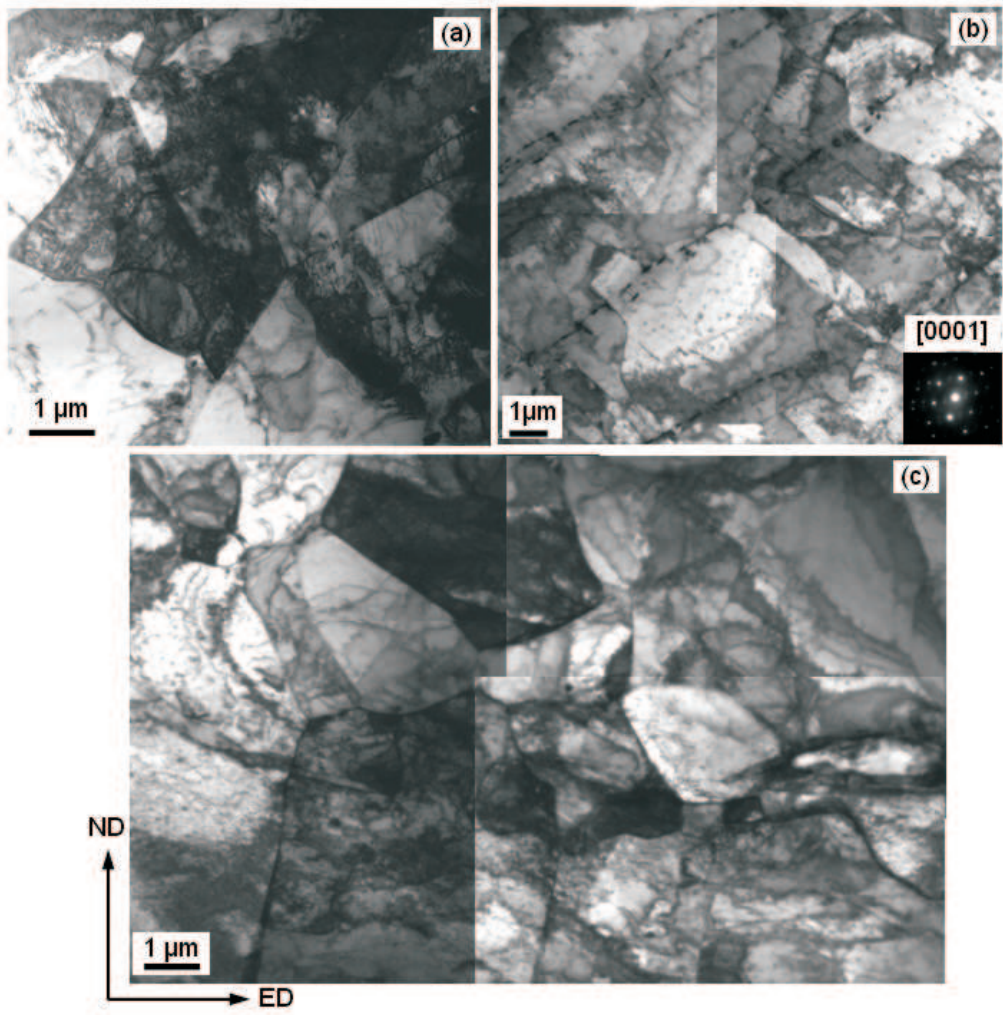

Fig. 7. Bright field TEM microstructures in samples plane strain compressed up to 0.8. Dislocation arrangements observed in samples deformed at: (a) 650°C and strain rate of $0.1s^{-1}$, (b) and (c) at 750°C and strain rate of $0.01s^{-1}$. Micrographs in (b) taken with [0001] beam direction. In (a) and (c) differently oriented grains are visible

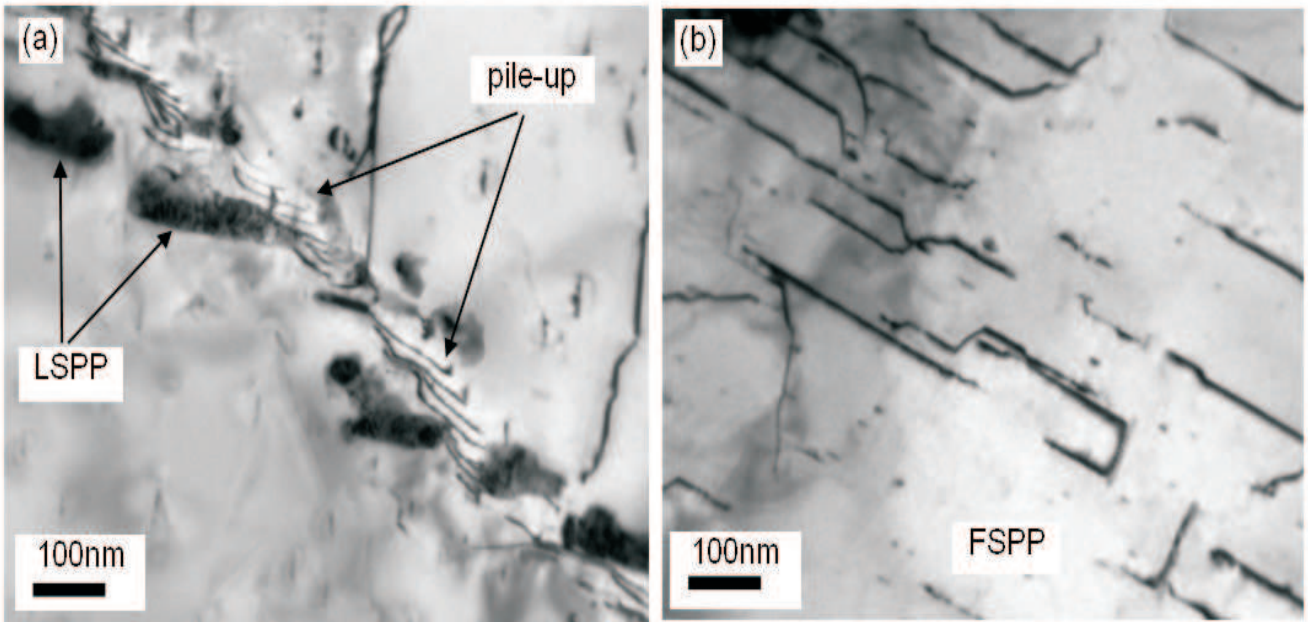

Fig. 8. Bright field TEM images showing interaction of dislocations with (a) large and (b) fine SPP, respectively. Pile-up of dislocations and dislocation pinning is to be noted. Samples deformed at 650°C and strain rate of 1.0 s^{-1} up to logarithmic strains of (a) 0.1 and (b) 0.2

In the case of plane strain deformed samples the observed microstructures do not show special differences with respect to these observed after uniaxial compression. The mixture of recovered/recrystallized grains and more or less dislocated areas were always detected, as is visible in Figs. 8a-c. As expected, the areas with high dislocation density were more frequently observed in samples deformed at lower temperature, i.e. 650°C.

The microstructures observed in the samples deformed at lower temperature and at the highest strain rates display the high volume fraction of fine and homogeneously distributed precipitates. In contrast, the microstructures observed in samples deformed at higher temperature and the lowest strain rate show, that most of the precipitate volume fraction consists of large and isolated precipitates, probably because low strain rate allowed for precipitates coarsening.

Both kinds of precipitates played also an important role in the dislocation motion, and in this way affects the deformation process. The interaction between moving dislocations and LSPP studied by TEM showed that some interactions occurred when dislocation lines cut through the particles, but most interactions ended as dislocation lines around the particles or pile-ups close to them (Fig. 8a). The pinning of dislocations is a typically observed interaction between fine particles and moving dislocations (Fig. 8b). This leads to the local stress concentration.

3.4. Local orientation measurements for twins identification

The twins were observed at both deformation temperatures, i.e. 650°C and 750°C. Nevertheless, it was very difficult to distinguish whether that mechanism resulted from the deformation or recrystallization twinning. Additionally, twinning was not uniform across the samples. That was probably due to the non-uniform stress and strain states resulting from frictional effects at the compression platens. A large grain size had also a favourable effect on twinning, although some twins were already present before the deformation. However, during warm compression their number and importance increase in unrecrystallized areas, practically independent of the applied conditions of deformation.

The twins were clearly observed even at OM and SEM scales in channel-die deformed samples. The areas close to corners of the sample were the privileged places for the twin appearance. However, inside other preferably oriented grains massive twinning was also observed (Fig. 9). The observations of deformed specimens under TEM reveal also different modes of twinning. All these modes were identified with the system of local orientation measurements in TEM, similar to that applied in SEM. In most cases the twinning was identified as the $\{10\bar{1}2\}\langle 10\bar{1}\bar{1}\rangle$ – type. Different aspects of twin formation are presented in Fig. 10. It is clear that the activity of twins could be stopped at the boundary of

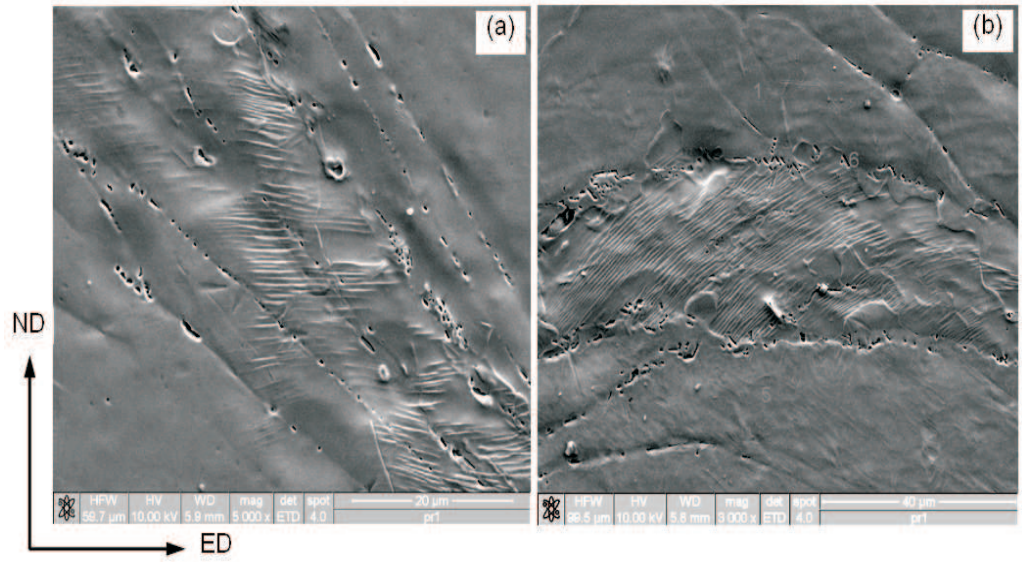

Fig. 9. Twins observed inside laths of α-grains. Section perpendicular to TD in plane strain deformed samples at: (a) 650°C and strain rate 0.1 s^{-1} and (b) 750°C and strain rate 0.01 s^{-1}. SEM analysis in secondary electrons

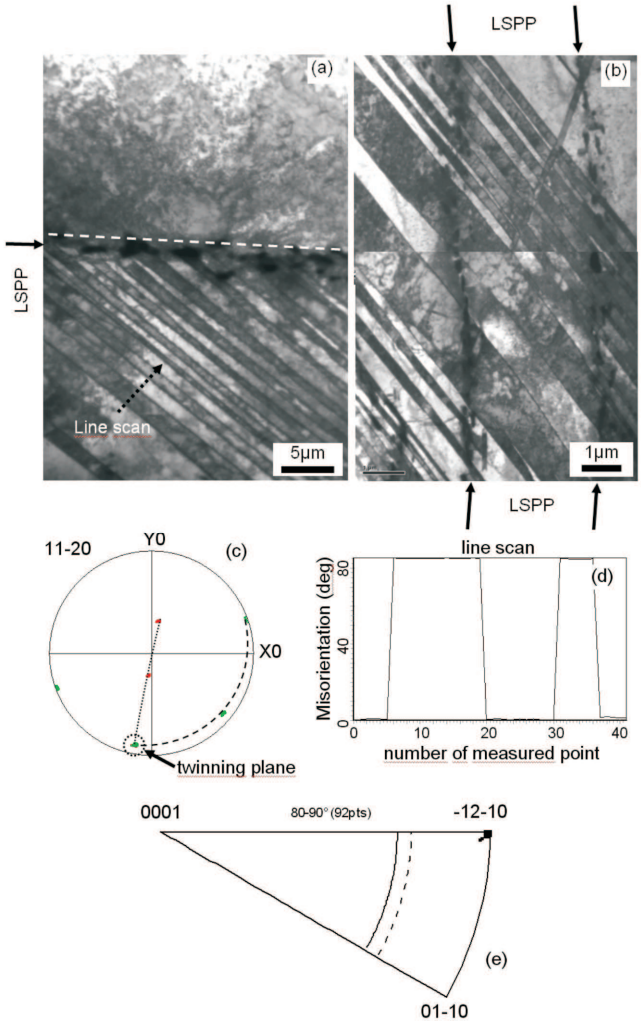

Fig. 10. TEM bright field images showing two aspects of twinning in Zry-4; (a) compact clusters of twins stopped at α-grain boundary and (b) twins crossing boundaries of the 'platelets' of α-grain. (c) $\{11\bar{2}0\}$ pole figure showing orientation of matrix and twin lamellae. (d) Misorientation profile calculated with respect to the first measured point lying inside matrix along line marked in (a). (e) Essential part of the misorientation axes distribution. Local orientation measurements in TEM with step size of 20 nm

α-grains (Fig. 10a) or could cross the lamellae of the same colony without any deviation in the shear direction (Fig. 10b). If the lamellae of the same colony had the same crystallographic orientations the lath boundaries within the colony did not constrain the different twinning system. For both presented cases the orientation of twins and matrix were similar and presented in Fig. 10c. The measured rotation angle (with respect to the first measured point) across the twinning plane was observed to be close to 84.0 - 84.5°, as presented in Fig. 10d, where a line scan along two platelets is showed. The misorientation axes grouped close to <11$\bar{2}$0> crystallographic direction (Fig. 10e).

Other analysed cases documented that several (up to 3) twin families were observed in the same colony, as presented in Fig. 11a. This bright field image shows twins, on different twinning planes, connected with second order pyramidal plane, i.e. the {1$\bar{1}$02} plane. The orientation of the matrix and all 3 variants of twins are shown in the stereographic projection presented in Figs. 11b and c. The misorientation angles calculated (with respect to the first measured point) along 3 line scans marked in the bright field image are presented in Figs. 12a-c, whereas the distribution of the misorientation axes is presented in Fig. 12d. The measured rotation angles from the matrix to twin positions are nearly the same and indicate the misorientation relation of 84.5°<1$\bar{1}$02>-type. It is evident that the twinning on one of the three {1$\bar{1}$02}-type plane leads to different variants of twins. All the above twins were of first generation, i.e. re-twinning of earlier twinned areas was absent.

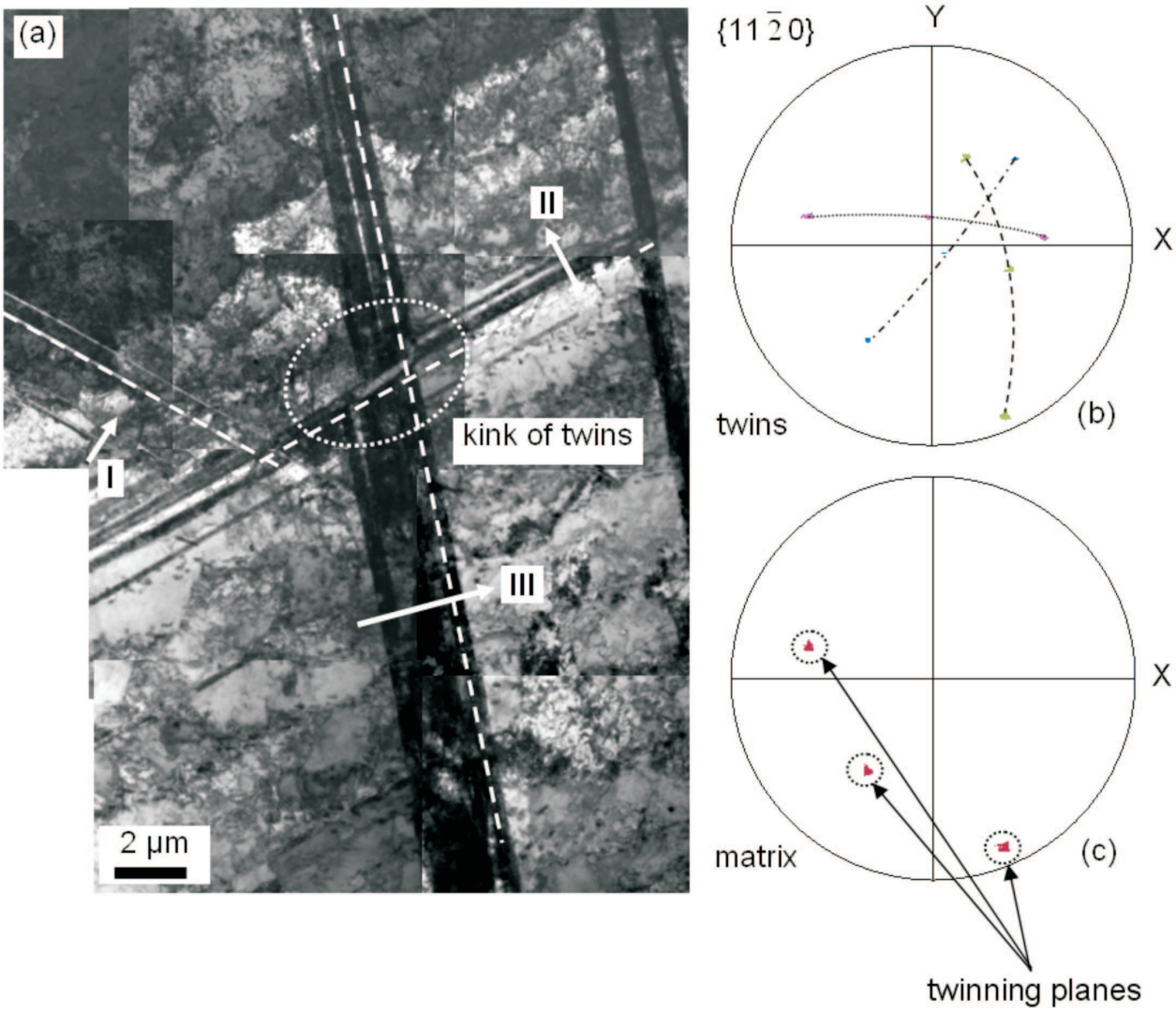

Fig. 11. TEM bright field image showing three families of {11$\bar{2}$0}-type twins, and corresponding {11$\bar{2}$0} pole figures showing (b) twins and (c) matrix positions; each family of twins nucleate from matrix on another twinning plane. Local orientation measurements in TEM with step size of 20 nm

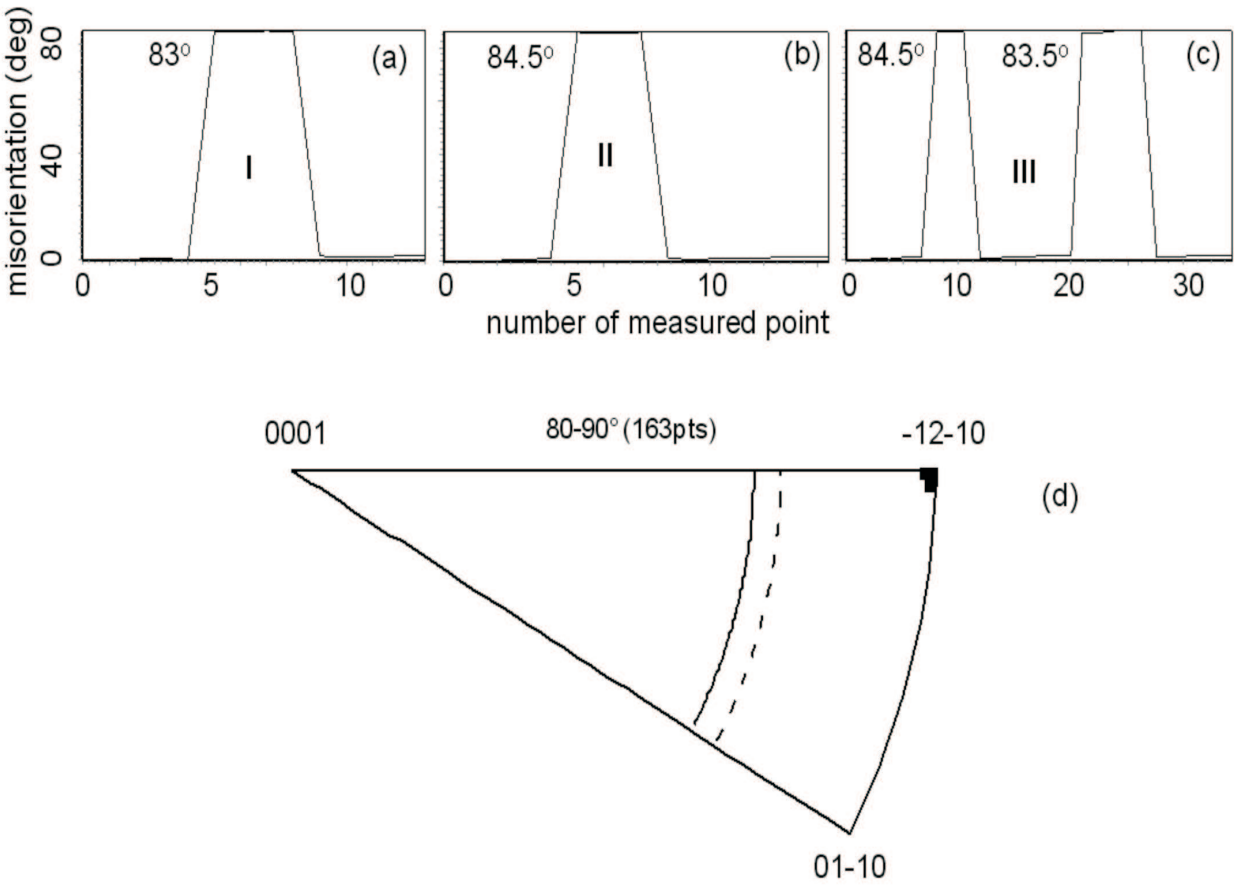

Fig. 12. (a)-(c) Misorientation line scans across twins presented in Fig. 11a and (d) corresponding essential part of misorientation axes distribution. Local orientation measurements in TEM with step size of 20 nm

More detailed analysis using systematic orientation mapping in TEM shows another possibility of twinning connected with the operation of $\{11\bar{2}1\}<11\bar{2}\bar{6}>$-type twinning system. However, the first of them, i.e. $\{1\bar{1}02\}$ was predominant.

4. Conclusions

The TEM was used to study the dislocation structure and morphology of SPP in Zry-4 compressed at 650°C and 750°C. Independently of its deformation mode, i.e. uniaxial or channel-die compressions, the observed dislocation microstructures were similar.

The typical microstructure of the Zry-4 alloy observed at TEM scale after warm deformation consisted of the α-phase and the intermetallic precipitates enriched in Fe and Cr. Two types of precipitates were observed. On one hand, the large SPP appeared mainly along the interlamellar boundaries within the α-grains and were observed only occasionally inside the platelets. In all analysed cases those particles were enriched in Fe and Cr. On the other hand, very fine, nearly homogeneously distributed particles situated inside platelets were observed. Both types of SPP played an important role in dislocation pinning.

Typical dislocation microstructure independently of applied deformation temperature was composed of a mixture of recrystallized and deformed areas. The efficiency of the recrystallization increases quite rapidly with increasing temperature or decreasing strain rate. However, only a small fraction of fully recrystallized sub-grains was observed.

Up to three different families of twins were observed independently of the applied deformation mode and strain rate or deformation temperature. However, the $\{1\bar{1}02\}$-type system of twins always prevailed.

REFERENCES

[1] C. Chauvy, P. Barberis, F. Montheillet, Microstructure transformation during warm working of β-treated lamellar Zircaloy-4 within the upper α-range. Mat. Sci. Eng. A, **431**, 59-67 (2006).

[2] C. Chauvy, Traitments thermomechaniques dans le haut domaine α du Zircaloy-4 trempe-β, PhD. Thesis,

Ecole Nationale Superieure des Mines de Saint Etienne (2005).

[3] J. Crépin, T. Bretheau, D. Caldemaison, Plastic deformation mechanisms of β-treated zirconium. Acta metall. mater. **43**, 3709-3719 (1995).

[4] J.W. Christian, S. Mahajan, Deformation twinning. Progress in Materials Science, **39**, 1-157 (1995).

[5] J.J. Fundenberger, M.J. Philippe, C.S. Esling, Mechanical twinning at high temperatures in some hexagonal alloys. Scripta Metall. et Mater. **24**, 1215-1220 (1990).

[6] C. Lemaignan, A.T. Motta, Zirconium Alloys in Nuclear Applications, Nuclear Engineering Department, The Pensylvania University, PA, 16802 (1992).

[7] R.E. Logé, J.W. Signorelli, Y.B. Chastel, M.Y. Perrin, R.A. Lebensohn, Sensitivity of αZy-4 high temperature deformation textures to the β-quenched precipitate structure and to recrystallization: application to hot extrusion. Acta Mater. **48**, 3917-3930 (2000).

[8] A.R. Massih, T. Anderson, P. Witt, M. Dahlbäck, M. Limbäck, Effect of quenching rate to β-to-α phase transformation structure in zirconium alloy. J. Nucl. Mater. **322**, 138-151 (2003).

[9] A. Morawiec, Automatic orientation determination from Kikuchi patterns, J. Applied Crystal. **32**, 788-798 (1999).

[10] H. Paul, TEM Orientation imaging in characterization of texture changes in fcc metals Advanced Engineering Materials, in print (2010).

[11] S.G. Song, G.T. Gray III, Structural interpretation of the nucleation and growth of deformation twins in Zr and Ti-I. Application of the coincidence site lattice (CSL) theory to twinning problems in H.C.P. structures. Acta metall. mater. **43**, 2325-2337 (1995).

[12] G. Tang, B.H. Choi, W. Kim, K-S. Jung, J.H. Lee, T.Y. Song, D.S. Shon, J.G. Han, Study of precipitation and dislocations in nitrogen implanted Zircaloy-4. Surface and Coatings Technology. **83**, 115-119 (1996).

[13] C.N. Tome, R.A. Lebensohn, U.F. Kocks, A model for texture development dominated by deformation twinning: application to zirconium alloys. Acta metall. mater. **39**, 2667-2680 (1991).

[14] W. Xiao, C. Ma, Study on the precipitates in Zircaloy-4 by Mössbauer spectroscopy. J. Nucl. Mater. **255**, 67-71 (1998).

Received: 30 June 2010.